Density functional theory investigation of the interaction of water with α-Al_2O_3 and α-Fe_2O_3 $(1\bar{1}02)$ surfaces: Implications for surface reactivity

Shela Aboud,[1,*] Jennifer Wilcox,[1] and Gordon E. Brown Jr.[2]

[1]*Department of Energy Resources Engineering, Stanford University, Stanford, California 94305 USA*

[2]*Department of Geological and Environmental Sciences, Department of Photon Science, and Department of Chemical Engineering, Stanford University, Stanford, California 94305-2115 USA*

(Received 17 September 2010; revised manuscript received 3 January 2011; published 17 March 2011)

Density functional theory calculations were performed in conjunction with *ab initio* thermodynamics, bond valence calculations, and density of states studies to investigate the chemical reactivity of α-Al_2O_3 and α-Fe_2O_3 $(1\bar{1}02)$ surfaces in a humid environment. Isostructural α-Fe_2O_3 $(1\bar{1}02)$ displays a much higher degree of surface reactivity with respect to water adsorption and aqueous heavy metal ions than α-Al_2O_3. The reason for these differences has not been fully explained. We have found that, while both metal oxides exhibit a similar stable $(1\bar{1}02)$ surface at and below room temperature, corresponding to a stoichiometric surface with the first layer of metal ions missing, the degree of hydroxylation of the surface oxygen atoms leads to differences in the atomic layer relaxation in α-Al_2O_3 $(1\bar{1}02)$ compared to α-Fe_2O_3 $(1\bar{1}02)$, which has also been confirmed previously by crystal truncation rod x-ray diffraction studies. Also in agreement with these experimental studies, we find the atomic layer spacing of the most energetically stable $(1\bar{1}02)$ Al_2O_3 surface is relatively insensitive to the inclusion of multiple layers of physisorbed water. This is in contrast to previously reported density functional theory studies of hydrated $(1\bar{1}02)$ α-Fe_2O_3 surfaces, the results of which are confirmed in this work, that a monolayer of water is required for good agreement with experimental measurements of the atomic layer relaxation. These changes in atomic spacing result in changes in electron charge distributions and in Lewis and Brønsted acid/base properties of surface sites, which influence the relative reactivities of the two surfaces. However, the higher reactivity of the hydrated $(1\bar{1}02)$ surface of α-Fe_2O_3 can be attributed mainly to the empty *d* states of the surface Fe atoms, which exhibit a first peak at $\sim$1 eV above the Fermi level and act as very strong Lewis acid sites. In comparison, the empty *p* states of Al in the hydrated $(1\bar{1}02)$ α-Al_2O_3 surface, which are $\sim$5 eV above the Fermi level, should be much less reactive to potential adsorbates.

DOI: 10.1103/PhysRevB.83.125407 PACS number(s): 68.47.Gh, 68.35.B−, 05.70.Np, 71.15.Mb

I. INTRODUCTION

Understanding the stability and reactivity of metal-oxide surfaces under humid conditions is of importance to a range of technical and environmental applications including microelectronics, high surface area catalyst supports, combustion by-products in the flue gas of coal-fired power plants, and the mobility of toxic metal ions in soils and groundwater aquifers. From an environmental standpoint, corundum (α-Al_2O_3) and hematite (α-Fe_2O_3) are of particular interest because of the use of the former as a model compound for Al-(oxyhydr)oxides present in the environment and the relative abundance of the latter in nature and its importance as a sorbent of aqueous cations, such as Hg(II), and oxoanions, such as $HAsO_4$.[1] In addition, these two compounds are isostructural in the bulk but show marked differences in chemical reactivity toward water and aqueous heavy metal and metalloid ions. Here, our focus is on explaining these differences in reactivity through a detailed computational investigation of the structural changes due to hydration and hydroxylation of α-Al_2O_3 and α-Fe_2O_3 surfaces.

The bulk corundum structure consists of a hexagonal close-packed array of oxygen atoms with metal ions occupying two-thirds of the available octahedral sites. Both α-Al_2O_3 and α-Fe_2O_3 can form two energetically stable surfaces, i.e., the (0001) or c-cut and the $(1\bar{1}02)$ or r-cut surface, which exhibit significantly different structural relaxations in the presence of water. As a result, the c-cut surface of α-Fe_2O_3 is much more reactive to the adsorption and dissociation of water compared with the r-cut surface of α-Fe_2O_3 and either of the α-Al_2O_3 surfaces.[1,2] Both crystal truncation rod (CTR) x-ray diffraction studies and density functional theory (DFT) calculations have found that the hydrated c-cut surface of α-Fe_2O_3 consists of two distinct domains, one in which surface hydroxyl groups are singly coordinated by iron(III) ions and one in which the surface hydroxyls are singly, doubly, and triply coordinated by iron(III) ions.[3] In comparison, the hydrated c-cut surface of α-Al_2O_3 has only surface hydroxyl groups doubly coordinated by aluminum ions.[4] This difference in surface hydroxyl group coordination may be a factor in the lower surface reactivity of the hydrated c-cut surface of corundum relative to the hydrated c-cut surface of hematite.[1,2] For example, the singly coordinated hydroxyl groups on the c-cut surface of hematite are thought to be responsible for the higher reactivity of this surface relative to the c-cut surface of corundum, which has only the doubly coordinated hydroxyl groups. In the case of the hydrated r-cut surfaces of both hematite and corundum, there are equal proportions of singly, doubly, and triply coordinated hydroxyl groups, yet the hydrated hematite r-cut surface is more reactive than the corresponding hydrated surface of corundum. There are also differences in the mode of binding of cations on the two surfaces. For example, aqueous U(VI) has been found to form dominantly inner-sphere bidentate complexes on the hydrated α-Fe_2O_3 r-cut surface and dominantly monodentate complexes on the hydrated α-Al_2O_3 r-cut surface.[5] In addition, aqueous Pb(II) ions form dominantly inner-sphere complexes on the hydrated α-Fe_2O_3 c-cut, α-Fe_2O_3 r-cut, and α-Al_2O_3 r-cut surfaces, but

they form dominantly outer-sphere complexes on the hydrated α-Al_2O_3 c-cut surface.[6,7] These differences in metal-ion surface complexation suggest different chemical reactivities of these different hydrated metal-oxide surfaces, which are likely due to differences in (1) metal ions (Al^{3+} vs Fe^{3+}), (2) surface relaxation in the presence of water (i.e., hydroxylation effects), (3) the acid/base properties of surface sites, and (4) interaction of physisorbed water with the surfaces.

Investigating the hydroxylation of the surface oxygen atoms and the structure of interfacial water on these oxide surfaces is the first step in elucidating the differences in relative reactivity between the α-Al_2O_3 and the α-Fe_2O_3 surfaces. Chemisorbed water dissociates on iron- and aluminum-oxide surface atoms and forms hydroxyl groups that contribute to the excess surface charge at the oxide/water interface.[8] The degree to which water and hydroxyl groups screen the surface charge and how this screening affects the corresponding reactivities of the surface sites are important. For instance, undercoordinated surface Al and Fe ions represent electron-accepting sites for water adsorption, whereas, after hydroxylation, the surface sites can exhibit weak base characteristics, ideal for metal-binding interactions.[2]

Because the mechanisms of metal-ion adsorption are sensitive to the nature of the surface and the surrounding environment, knowledge of the physical structure of the metal-oxide/aqueous solution interface under relevant environmental conditions is essential for understanding the reactivities of the metal-oxide surfaces. In addition to surface hydroxyl groups, physisorbed water on the surface should also play a role in surface reactivity. Water molecules will tend to orient in such a way as to shield the charged hydroxyl groups, thereby decreasing the polarizability of the water and reducing the dielectric constant of water near the surface. The interfacial dielectric constant is difficult to measure experimentally, and values ranging from 6 to 53 (compared to 78 in bulk water) have been suggested for water in contact with both α-Al_2O_3 and α-Fe_2O_3.[9] High-resolution specular x-ray reflectivity experiments[10] showed that approximately two layers of water are ordered on the hydrated α-Fe_2O_3 and α-Al_2O_3 r-cut surfaces, beyond which the dipoles of water molecules are randomly oriented. Furthermore, in an electrolytic solution, ions will also contribute to screening the surface charges, resulting in changes in the surface potential and acting to modify the electrical double layer. Whether an ion interacts with the surface via inner-sphere or outer-sphere complexation (or both simultaneously[11]) depends on a complicated interaction between these surface hydroxyl groups and the corresponding induced electric field from the charged species, all of which ultimately depend on the geometric and electronic structures of the given surface.

Although CTR diffraction measurements provide information about the average structural environments of oxygen and metal ions in the top 10 Å of metal-oxide surfaces, they are not able to resolve the positions of hydrogen atoms. However, the approximate positions of the hydrogen atoms associated with oxygen atoms in the top 10 Å of hydrated metal-oxide surfaces can be inferred using bond valence (BV) theory and Pauling's electrostatic valence rule.[12] The position of hydrogen atoms can also be predicted from first-principle DFT calculations, and such calculations can also address how the protonation of various undercoordinated oxygen species in the metal-oxide surface region stabilizes the overall surface structure. In addition, given that the relative stabilities of these surfaces are sensitive to the pressure and temperature conditions of the surrounding environment, DFT calculations can be combined with *ab initio* thermodynamics to extrapolate the experimental findings for other relevant conditions. DFT can also be used to understand the interaction of the first layers of water molecules with the metal-oxide surfaces.[13]

CTR x-ray diffraction studies of α-Fe_2O_3 and α-Al_2O_3 r-cut surfaces show significant differences in the amount of relaxation, with much less relaxation found for α-Fe_2O_3.[14,15] A comprehensive investigation of the stability of the hydrated α-Fe_2O_3 r-cut surface was performed by Lo *et al.*[13] using DFT and *ab initio* thermodynamics and showed reasonable structural agreement with an experimental CTR x-ray diffraction study[15] when a monolayer of water was included in the simulation domain. Few, if any, DFT calculations have been performed that include multiple layers of water on surfaces. The highly polarized nature of the first several layers of the physisorbed water molecules on the r-cut α-Fe_2O_3 and α-Al_2O_3 surfaces allows us to examine the influence of these multiple layers on the structure and the corresponding changes in reactivity.

In this paper, DFT, *ab initio* thermodynamics, BV and density of states (DOS) calculations were used to investigate the mechanisms responsible for the atomic layer relaxation and the impact that these relaxations have on the reactivity of the hydrated α-Al_2O_3 r-cut surface. Comparisons were then made with the hydrated α-Fe_2O_3 r-cut surface to determine how geometric and electronic contributions translate into differences in reactivity between these two metal oxides. Although CTR x-ray diffraction studies of α-Al_2O_3 and α-Fe_2O_3 r-cut surfaces showed both to have an energetically stable bihydroxylated surface structure,[14,15] the DFT results predict an additional stable monohydroxylated surface structure for the hydrated α-Al_2O_3 r-cut surface in which hydroxylation extends more deeply into the surface than for the bihydroxylated surface or the hydrated α-Fe_2O_3 r-cut surface. The presence of these hydrogen atoms in the subsurface region of the monohydroxylated surface significantly increases the BV of hydroxylated oxygen atoms, leading to a higher degree of layer relaxation. BV analysis also showed an increase in the reactivity of physisorbed water when more than two layers were included in the simulation. An increase in the Brønsted acidity of the physisorbed water molecules when three layers of water are included stems from the influence of the neighboring hydrogen bonds, and in a dynamic system the water molecules will reorient themselves to minimize high BV values.

II. COMPUTATIONAL METHODOLOGY

A. Electronic structure calculations

DFT calculations were performed using the Vienna *ab initio* Simulation Package (VASP)[16] with the projector augmented wave method.[17] Electron exchange-correlation functionals were represented with the generalized gradient approximation using the model of Perdew, Burke, and Ernzerhof.[18] A plane-wave expansion cutoff of 450 eV was applied, and the surface

TABLE I. Equilibrium hexagonal unit cell parameters calculated with DFT compared with experimental values and values from other computational studies.

	a (Å)	b (Å)	c (Å)	M (μ_B)
α-Al_2O_3—this work	4.807	4.807	13.122	
α-Al_2O_3—Exp[a]	4.7589	4.7589	12.991	
α-Al_2O_3—Exp[b]	4.757	4.757	12.988	
α-Al_2O_3—DFT[c]	4.7792	4.7792	13.049	
α-Al_2O_3—DFT[d]	4.7877	4.7877	13.075	
α-Al_2O_3—DFT[e]	4.823	4.823	13.111	
α-Fe_2O_3—this work	5.031	5.031	13.753	3.5
α-Fe_2O_3—Exp[f]	5.038	5.038	13.772	
α-Fe_2O_3—Exp[g]	5.0346	5.0346	13.752	4.6–4.9
α-Fe_2O_3—DFT[h]	5.007	5.007	13.829	3.4
α-Fe_2O_3—DFT[i]	5.05	5.05	13.81	3.6

[a]See Ref. 21.
[b]Reference 22.
[c]Reference 23.
[d]Reference 24.
[e]See Ref. 7.
[f]See Ref. 21.
[g]See Ref. 25.
[h]See Ref. 26.
[i]See Ref. 13.

Brillouin zone integration was calculated using a Γ-centered $5 \times 5 \times 5$ ($5 \times 5 \times 1$ for the surface) Monkhorst-Pack mesh.[19] Methfessel and Paxton[20] Gaussian smearing of order 1 with a width of 0.2 eV was used to accelerate convergence of the total-energy calculations. Geometric optimization was performed using the conjugate-gradient algorithm until the absolute value of the forces on unconstrained atoms was less than 0.03 eV/Å.

The initial bulk α-Al_2O_3 and α-Fe_2O_3 structures for the VASP simulations were obtained from the experimentally measured[21] atomic coordinates consisting of a 20-atom hexagonal unit cell (12 Al/Fe and 18 O atoms). The simulated equilibrium lattice parameters were found by changing the length of each side of the unit cell while holding the other two sides fixed to find the set of lattice parameters that minimize the total free energy of the system. The resulting parameters for a, b, and c are shown in Table I along with the experimental values and the results of other DFT calculations on these structures. The total unit cell volumes were found to increase by 1% for α-Al_2O_3 and to decrease by 0.1% for α-Fe_2O_3, which match very well with the results of other DFT calculations. Although α-Fe_2O_3 is antiferromagnetic under the conditions of interest, the magnetic moment of the individual Fe atoms has been measured and has been found to be on the order of $4.6 - 4.9\mu_B$.[22–25] The magnetic moment of individual Fe atoms in α-Fe_2O_3 was found to be $3.5\mu_B$ in the current DFT work. Previous DFT studies of $3d$ metal oxides have found a similar underestimation of magnetic moments, which has been attributed to an overestimation of the mixing of the O $2p$ and Fe $3d$ states or to an overestimation of the experimentally determined magnetic moments from neutron diffraction measurements due to distortions of the magnetic form factor stemming from this same mixing, which changes the purely ionic picture of the metal oxide.[26] The layer spacing along the $[1\bar{1}02]$ direction was also calculated and compares well with CRT x-ray diffraction measurements by Trainor *et al.*[14] for the hydrated α-Al_2O_3 r-cut surface and by Tanwar *et al.*[15] for the hydrated α-Fe_2O_3 r-cut surface as shown in Fig. 1, where the difference between the DFT results and experiment is shown in parentheses. The maximum difference between calculated DFT values and experiment is approximately 1% for α-Al_2O_3 r-cut and 3.3% for α-Fe_2O_3 r-cut.

The $(1\bar{1}02)$ surfaces were constructed by cleaving the bulk oxide along the $(1\bar{1}2)$, (110), and $(1\bar{1}1)$ planes. Along the $[1\bar{1}2]$ direction, a double-sided slab was formed with 20–24 atomic layers, which is thick enough to maintain the bulk structure in the center region of the slab. The two sides of the slab are identical to ensure symmetric dipole layers at the surface, and a vacuum region of approximately 30 Å was used to isolate the slab from its periodic images. Test structures with 30 atomic layers and a 40-Å vacuum layer changed the surface free energy by less than 0.5% compared to the system with 20 atomic layers and 30-Å vacuum. The parameters are also consistent with previous DFT studies of α-Fe_2O_3 r-cut that used 16–22 layers and a 20-Å vacuum region.[13]

B. *Ab initio* thermodynamics

The stability of a given oxide surface was determined as a function of temperature and pressure by comparing the relative surface free energies, as defined in Eq. (1),[27]

$$\gamma = \frac{1}{2A}\left[G_{\text{slab}} - \frac{N_{\text{M}}}{2}g_{\text{M}_2\text{O}_3} - \left(N_{\text{O}} - \frac{3N_{\text{M}}}{2} - \frac{N_{\text{H}}}{2}\right)\mu_{\text{O}} - \frac{N_{\text{H}}}{2}\mu_{\text{H}_2\text{O}}\right], \quad (1)$$

where A is the area of the slab, G_{slab} is the Gibbs free energy of the slab, $g_{\text{M}_2\text{O}_3}$ is the Gibbs free energy of the metal-oxide bulk per Al_2O_3 or Fe_2O_3 formula unit, μ_O is half the chemical potential of the gas-phase O_2 molecule, $\mu_{\text{H}_2\text{O}}$ is the chemical potential of the gas-phase H_2O molecule, and N_M,N_O, and N_H refer to the number of metal, oxygen, and hydrogen atoms in the slab, respectively.

The configuration free energy is accounted for indirectly through the use of a screening approach in which the relative differences among the surface free energies of all the slabs were used to determine the optimal surface configuration at the given thermodynamic conditions. Neglecting contributions from pressure, the Gibbs free energy can then be approximated by the energy at constant volume, calculated with DFT, and the vibrational free energy. The vibrational free energy of the slab consists of a contribution from the bulk phonon modes and the surface and adsorbate modes. It is assumed that the bulk phonon modes do not change with the creation of the slab or by the adsorption of oxygen and hydrogen atoms on the surface, and, therefore, the bulk phonons in the slab will cancel with the vibrational portion of the bulk free energy. In addition, Sun *et al.*[28] have shown that the change in energy due to the vibrational modes of excess surface oxygen atoms on an oxide surface is within the computational error of the DFT approach.

In this paper, the only contribution to the vibrational free energy is from the hydrogen atoms of the bound water and

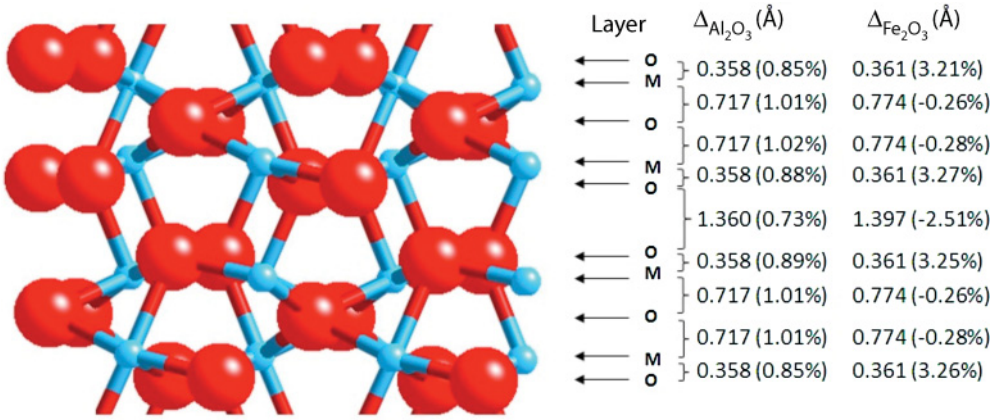

FIG. 1. (Color online) Calculated layer spacing in the bulk α-Al_2O_3 and α-Fe_2O_3 structures along with the percent difference relative to experimental values (shown in parentheses) (from Trainor *et al.*[14] and Tanwar *et al.*,[15] respectively). The M refers to either Al or Fe.

hydroxyl groups. The vibrational frequencies were calculated by starting with the equilibrated structures and by fixing all of the atomic coordinates except those of hydrogen atoms on one side of the slab. Each hydrogen atom was then displaced from its equilibrium position by 0.01 Å in both the positive and the negative directions. The other hydrogen atoms were allowed to relax until a new minimum energy configuration was determined. The vibrational frequencies were then extracted by diagonalizing the mass-weighted Hessian matrix, which is constructed with the second derivatives of the energy using the central difference method. The temperature and pressure dependence of the gas-phase chemical potentials were obtained from the National Institute of Standards and Technology-Joint Army-Navy-Air Force (NIST-JANAF) thermochemical tables.[29]

C. Bond Valence Analysis

The bond valence (BV) model is an empirical measure of Pauling's valence sum rule[12] relating the electrostatic bond strengths around each ion in a structure to its valence number. The amount that the total BV of an ion differs from the ion's valence number then provides a direct measure of the under- or overcoordination of the ion in the structure, ultimately providing information about the reactivity of that atomic site. For example, oxygen atoms having a total BV equal to 2 valence units (v.u.) will not be reactive, whereas, undercoordinated surface oxygen atoms with a total BV less than 2 v.u. will act as Brønsted bases wanting to bind with a proton in the surrounding environment. Overcoordinated oxygen atoms with a total BV greater than 2 v.u. will ultimately be unstable and if bound to a proton, will act as a strong Brønsted acid to reduce the total BV. The contribution to the total BV from each neighboring ion is fit to an empirical formula, which for Al_2O_3 and Fe_2O_3, is given by the expression[30]

$$s_{M-O} = \exp\left(\frac{R_O - R_{M-O} - \Delta R^{DFT}_{M-O}}{0.37}\right) \quad (2)$$

where M is an Al or Fe atom and the experimentally determined values for R_O are 1.651 and 1.759 Å for Al_2O_3 and Fe_2O_3, respectively. In this paper, an additional term, ΔR_{DFT}, was used to correct for the DFT optimization of the unit cell resulting in a change in the equilibrium bond length between ions. The total BV of a particular ion, i, is given by summing the individual contributions from all the bonded neighboring ions using Eq. (3),

$$\text{Total BV} = \sum \frac{\text{charge}}{\text{coordination}} = \sum_j s_{i-j} \quad (3)$$

The DFT correction term of $\Delta R^{DFT}_{Al-O} = 0.029$ and $\Delta R^{DFT}_{Fe-O} = 0.011 Å$ results in the total BV for Al and Fe of 3 and the total BV for O of 2 in the bulk structures. The contribution to the total BV for the hydroxyl groups was calculated using the following equation:[31]

$$s_{O-H} = \frac{0.241}{R_{O-H} - 0.677 - \Delta R^{DFT}_{O-H}}, \quad (4)$$

where R_{O-H} is the O-H bond distance. The DFT correction to the total BV of the hydrogen bond is $\Delta R^{DFT}_{O-H} = 0.055 Å$ and is calculated by simulating a single water molecule in a $10 \times 10 \times 10 Å$ box and by normalizing the total BV to 1 v.u. Without the correction, the total BV of the hydrogen atom is unrealistically large with a total BV of 1.63 v.u.

D. Bader charge and magnetic moments

The electronic charge distribution from the DFT calculations was partitioned and was assigned to the individual atoms using Bader charge analysis.[32] Using this approach, the continuous electron density (including both the valence and the core electrons) is partitioned into regions bounded by the minima of the charge density and then is assigned to a given atom. The magnetic moments of the individual atoms in α-Fe_2O_3 were calculated by subtracting the electron density with different spins and then partitioning this magnetic moment distribution using the Bader volumes in an approach analogous to that used for the charge density.

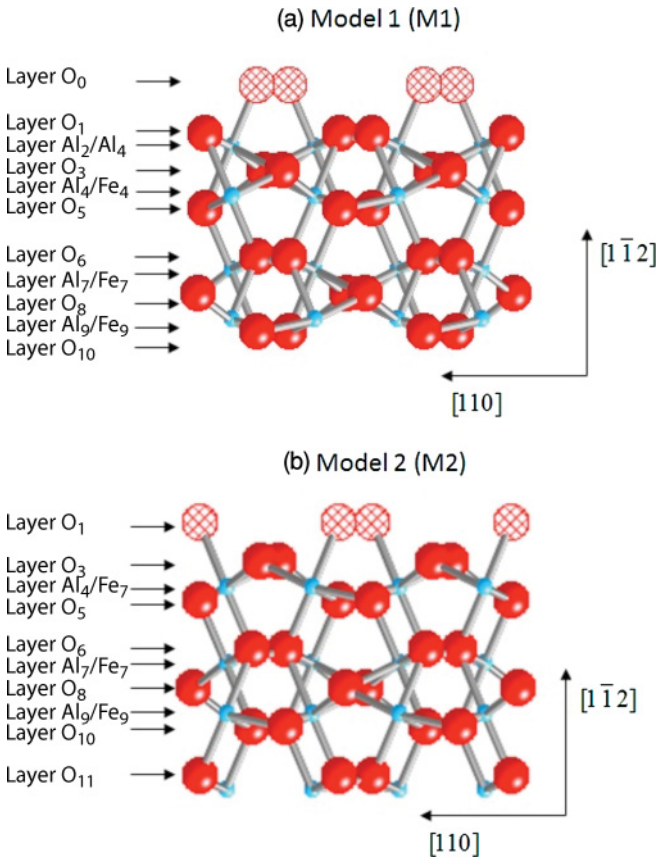

FIG. 2. (Color online) Two stable oxygen terminated surfaces for the r-cut surfaces of α-Al_2O_3 and α-Fe_2O_3 denoted (a) M1 for oxygen added to the stoichiometric and (b) M2 for the surface missing the top layer of metal atoms. The hatched atoms denote the oxygen atoms terminating the surface.

III. RESULTS AND DISCUSSION

A. Optimized geometric structure

Two stable configurations of the oxygen-terminated r-cut surfaces of the α-Al_2O_3 and α-Fe_2O_3 structures were found, as illustrated in Fig. 2. The configuration, denoted model 1 (M1) in Fig. 2(a), corresponds to O atoms adsorbed directly to the cation sites in the ideal stoichiometrically terminated surface, whereas, model 2 (M2) shown in Fig. 2(b) corresponds to the ideal stoichiometrically terminated surface with the first layer of cations removed. Results of CTR x-ray diffraction measurements of the hydrated α-Al_2O_3[14] and α-Fe_2O_3[15] r-cut surfaces at room temperature indicate that the M2 surface configuration is the most probable one. For the r-cut surface, the topmost oxygen atoms of both model surfaces are only singly coordinated (Fig. 2). The next layer of oxygen atoms is doubly coordinated, and in the case of the missing top cation of the M2 surface, the third-layer oxygen atoms are triply coordinated. In this paper, simulations were carried out for a variety of hydroxyl configurations for these undercoordinated oxygen atoms. Monohydroxylation and bihydroxylation of the topmost surface oxygen atoms were considered, and single hydroxylation of the next two layers of oxygen atoms was simulated. Comparisons were then made using *ab initio* thermodynamics to determine which surface structure is the most energetically stable under various temperature and pressure conditions.

B. Surface free energies derived from *ab initio* thermodynamics

Figure 3 shows a plot of the absolute minimum surface free energy as a function of temperature and oxygen partial pressure along with the atomic configuration of the corresponding r-cut surface structure for α-Al_2O_3. At high temperatures, the hydrogen atoms are not stable on the surface, and the M1 clean stoichiometric surface (M1 bulk), which has no

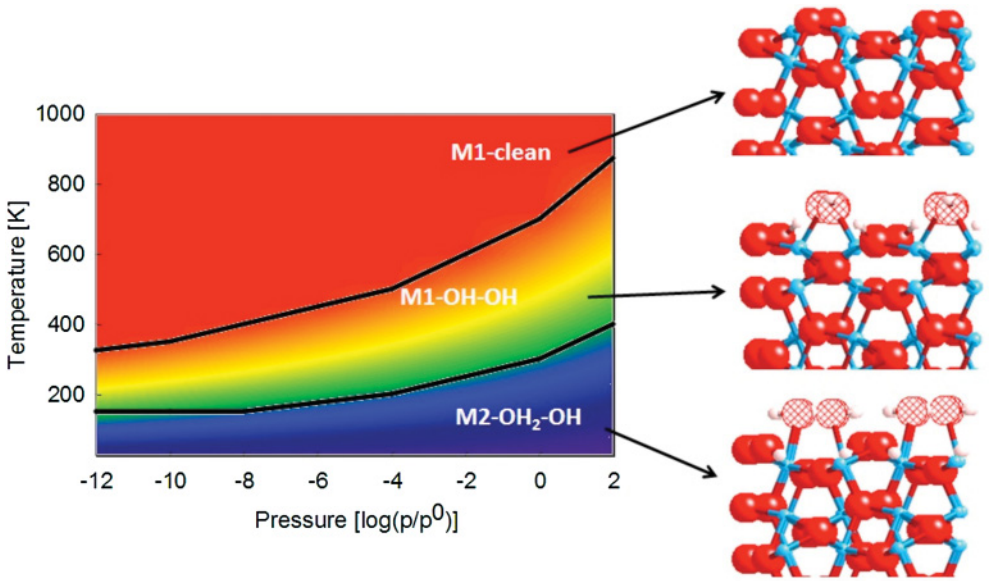

FIG. 3. (Color online) Minimum surface free energy as a function of temperature and oxygen partial pressure. The color scheme denotes the value of the minimum free energy from low (−60 meV/Å) in blue to high (102 meV/Å) in red. Water and oxygen partial pressures are equal. Corresponding structures are shown on the right. The hatched atoms denote the oxygen atoms terminating the surface.

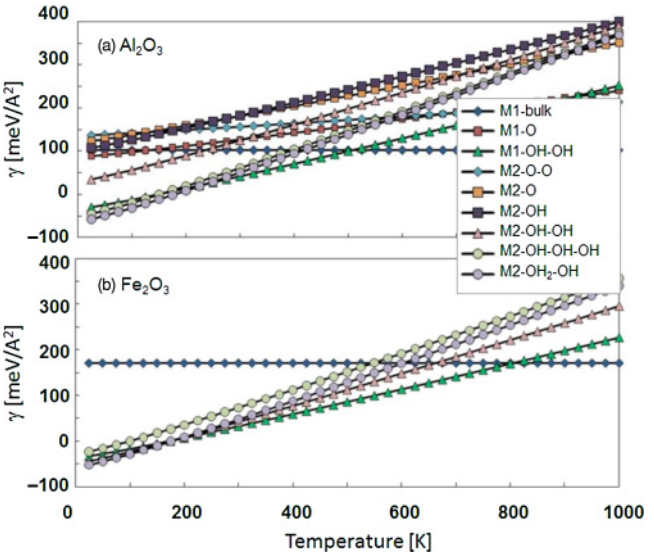

FIG. 4. (Color online) Surface free energy as a function of temperature for $pO_2 = 10 - 8$Torr and $pH_2O = 1.6$Torr for the most energetically stable nonhydrated (a) $\alpha - Al_2O_3$ and (b) $\alpha - Fe_2O_3$ r-cut surface structures.

hydroxyl groups, is the most energetically favorable. At room temperature and below over most of the pressure range (-12 to $\sim 1 \log p/p^0$) the M1-OH-OH surface is the most stable in which the first two layers of oxygen atoms are hydroxylated. However, the M2-OH_2-OH surface termination with missing Al atoms becomes stable at room temperature at $\log p/p^0 > \sim 1$. The M2-OH_2-OH surface has bihydroxylated top oxygen atoms and a second layer of hydroxylated oxygen atoms. This bihydroxylated surface has also been confirmed to be the most energetically stable of the α-Fe_2O_3 r-cut surfaces at low oxygen chemical potentials through the DFT calculations of Lo *et al.*[13]

Figure 4 shows plots of the surface free energy of the r-cut (a) α-Al_2O_3 and (b) α-Fe_2O_3 surfaces as a function of temperature for a partial pressure of oxygen (p_{O_2}) and water (p_{H_2O}) of 10^{-8} and 1.6 Torr, respectively, which correspond to the values from the CTR measurements. Although the M2-OH_2-OH surface has the minimum free energy for both the α-Al_2O_3 and the α-Fe_2O_3 r-cut surfaces at low temperatures, it is important to note that the next stable M2 surface in which the top-layer oxygen atoms are monohydroxylated is only approximately 11.3 and 7.4 meV/Å^2 higher in energy at 0 K for α-Al_2O_3 and α-Fe_2O_3, respectively. These differences are arguably within the computational error of DFT. However, it is also worth noting that DFT predicts that different monohydroxylated surfaces are more stable for α-Al_2O_3 than for α-Fe_2O_3. For α-Al_2O_3, the monohydroxylated r-cut surface, with the second and third layers of oxygen atoms hydroxylated (M2-OH-OH-OH), is more stable than the surface with only the second layer of oxygen atoms hydroxylated (M2-OH-OH). The opposite trend is found for α-Fe_2O_3 and the M2-OH-OH surface where hydroxylation penetrating deepest into the bulk is less energetically stable. Because the relative differences in energy between the most stable M2 surfaces, for both α-Al_2O_3 and α-Fe_2O_3, are very close in value, it is difficult to predict the most likely hydrogen configuration using only the results of the *ab initio* thermodynamics calculations. In Sec. III C, the experimentally determined metal and oxygen atomic coordinates from the CTR x-ray diffraction measurements will be compared to the most energetically stable simulated structures in order to deduce which hydrogen configurations result in the best match with experiment.

C. Differences in surface relaxation of α-Al_2O_3 and α -Fe_2O_3

The atomic layer spacing and percent relaxation in the direction perpendicular to the α-Al_2O_3 and α-Fe_2O_3 r-cut surfaces are reported in Tables II and III, respectively, for the three most stable hydroxylated M2 structures (M2-OH-OH, M2-OH-OH-OH, and M2-OH_2-OH), along with the structure from the CTR x-ray diffraction measurements. Although the CTR x-ray diffraction experiments predict the M2 surface as the most probable structure for the hydrated r-cut α-Al_2O_3 and α-Fe_2O_3 surfaces, the results show significant differences in relaxation behavior. The atoms in the top surface layers of α-Al_2O_3 experience more relaxation with respect to the bulk positions than surface atoms in α-Fe_2O_3 under the same environmental conditions. These differences in layer relaxation extend as much as nine to ten layers into the bulk region (Tables II and III). The protonation states of the singly, doubly, and triply coordinated oxygen atoms directly affect both the type and the extent of relaxation.

In the case of α-Al_2O_3, the hydroxyl configuration that results in a layer spacing most closely matched the experimental values corresponding to the M2-OH-OH-OH surface, which

TABLE II. Atomic layer relaxation of M2 r-cut surfaces for α-Al_2O_3. The percent relaxation of the surface layer compared to the bulk is shown in parentheses.

Layer	α-Al_2O_3 M2 Ref. 14 (Å)	α-Al_2O_3 M2-OH-OH (Å)	α-Al_2O_3 M2-OH-OH-OH (Å)	α-Al_2O_3 M2-OH_2-OH (Å)
$\Delta(O_1\text{-}O_3)$	1.460 (36.9%)	1.156 (7.5%)	1.245 (15.6%)	1.425 (32.3%)
Δ (O_3-Al_4)	0.368 (−48.3%)	0.532 (−25.8%)	0.441 (−38.5%)	0.703 (−1.9%)
Δ (Al_4-O_5)	0.465 (31.3%)	0.590 (64.7%)	0.592 (64.5%)	0.351 (−2.5%)
Δ (O_5-O_6)	1.200 (−11.0%)	1.241 (−8.8%)	1.267 (−6.9%)	1.367 (0.5%)
Δ (O_6-Al_7)	0.403 (13.7%)	0.362 (1.2%)	0.439 (22.0%)	0.361 (0.4%)
Δ (Al_7-O_8)	0.781 (9.8%)	0.744 (3.8%)	0.680 (−5.2%)	0.730 (1.8%)
Δ (O_8-Al_9)	0.641 (−9.8%)	0.675 (−5.9%)	0.681 (−5.0%)	0.715 (−0.2%)
Δ (Al_9-O_{10})	0.344 (−3.0%)	0.376 (5.0%)	0.375 (4.3%)	0.355 (−1.3%)

TABLE III. Atomic layer relaxation of M2 r-cut surfaces for α-Fe_2O_3. The percent relaxation of the surface layer compared to the bulk is shown in parentheses.

Layer	Fe_2O_3 M2 Ref. 15 (Å)	Fe_2O_3 M2-OH-OH (Å)	Fe_2O_3 M2-OH-OH-OH (Å)	Fe_2O_3 M2-OH_2-OH (Å)
$\Delta(O_1\text{-}O_3)$	1.259 (11.8%)	1.020 (−10.2%)	1.244 (9.9%)	1.521 (34%)
Δ (O_3-Fe_4)	0.691 (−10.9%)	0.611 (−21.1%)	0.532 (−31.2%)	0.787 (1.7%)
Δ (Fe_4-O_5)	0.380 (8.4%)	0.579 (60.5%)	0.548 (51.9%)	0.352 (−2.5%)
Δ (O_5-O_6)	1.411 (−1.5%)	1.199 (−14.4%)	1.309 (−6.5%)	1.409 (0.64%)
Δ (O_6-Fe_7)	0.365 (4.2%)	0.421 (16.6%)	0.505 (40%)	0.354 (−2.1%)
Δ (Fe_7-O_8)	0.776 (0.0%)	0.850 (9.88%)	0.702 (−9.3%)	0.794 (2.7%)
Δ (O_8-Fe_9)	0.769 (−1.0%)	0.764 (−1.27%)	0.739 (−4.5%)	0.780 (0.8%)
Δ (Fe_9-O_{10})	0.350 (0.0%)	0.335 (−7.2%)	0.370 (2.6%)	0.357 (−1.1%)

has a monohydroxylated top surface oxygen atom and two additional layers of hydroxylated oxygen atoms extending into the bulk. Although this configuration is the closest match, there are several significant differences between the DFT predictions and the experimental results.

The main discrepancy between the M2-OH-OH-OH theoretical predictions and the experiment is the relaxation between the seventh and eighth atomic layers, corresponding to Al and O atoms, respectively, and is denoted by $\Delta(Al_7\text{-}O_8)$ in Table II. This layer spacing is found to decrease by −5.2% from the DFT calculations, but experimentally, it was found to increase by 9.0%. However, it is important to note that, although the direction of the relaxation is different (contraction in the DFT case and expansion in the experiment), the absolute difference is small, and a change in the position of the O_8 atom by less than 0.1 Å in either the experimental measurements or the DFT results would make the percent relaxations match. Additionally, the magnitude of the relaxation of the M2-OH-OH-OH surface spacing calculated with DFT is more than a factor of 2 higher for $\Delta(Al_4\text{-}O_5)$ and a factor of 2 lower for $\Delta(O_1\text{-}O_3)$ compared to experiment. It is possible that, in the experimental work, the surface is not entirely homogeneous, and the CTR measurements include multiple hydroxylation configurations on the surface.

Consistent with previous DFT studies,[13] the geometry of the experimentally determined surface is not well captured by any of these DFT hydroxyl configurations for α-Fe_2O_3. This previous work, the results of which are confirmed here (see Sec. III F), found that the predicted atomic layer relaxation of the M2-OH_2-OH surface of α-Fe_2O_3 matched experimental values only when a monolayer of physisorbed water molecules was included in the simulation. As discussed in detail in Sec. III F below, the effect of physisorbed water on the layer relaxation of the α-Al_2O_3 r-cut surfaces was also examined, but it did not significantly change the results or the geometric structure of the M2-OH-OH-OH surface, which is in closest agreement with the CTR diffraction results.

D. Reactivity: Lewis and Brønsted acid-base properties of r-cut surfaces

One of the principal goals of this paper is to use DFT simulations of the various hydroxylated α-Al_2O_3 and α-Fe_2O_3 r-cut surfaces to understand how structural differences affect differences in intrinsic reactivity of these oxide surfaces. The reactivity of the surfaces can be characterized by the strength of both Lewis and Brønsted acid-base sites, which can be understood through DOS and BV analysis.

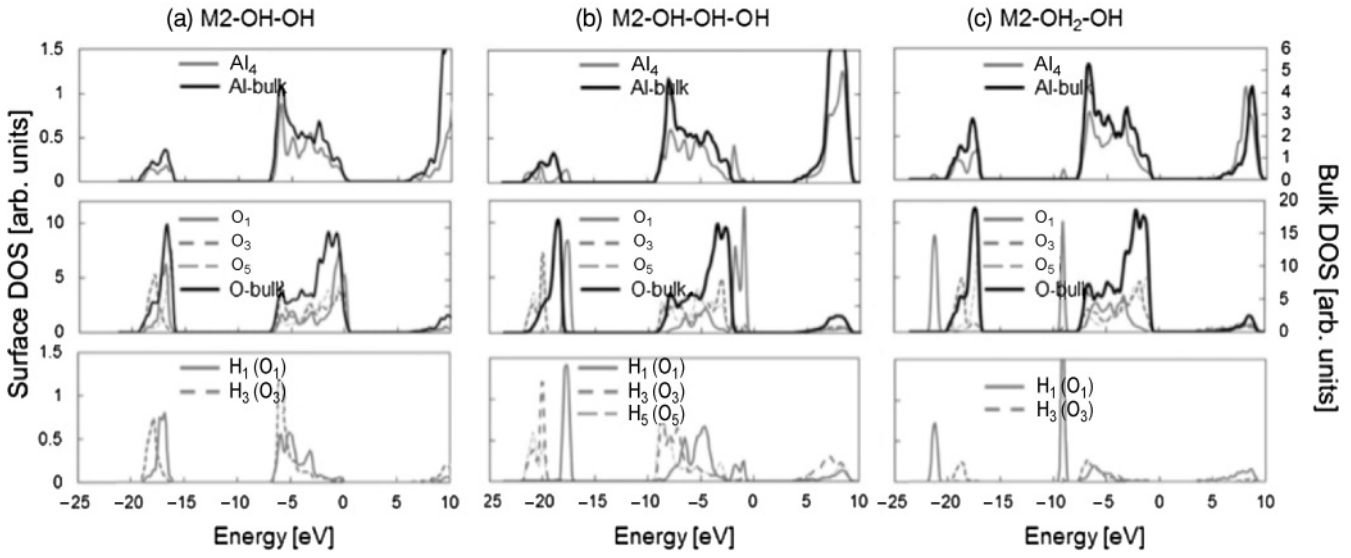

FIG. 5. DOS for the most stable hydroxylated M2 r-cut surfaces of α-Al_2O_3, for (a) M2-OH-OH, (b) M2-OH-OH-OH, and (c) M2-OH_2-OH.

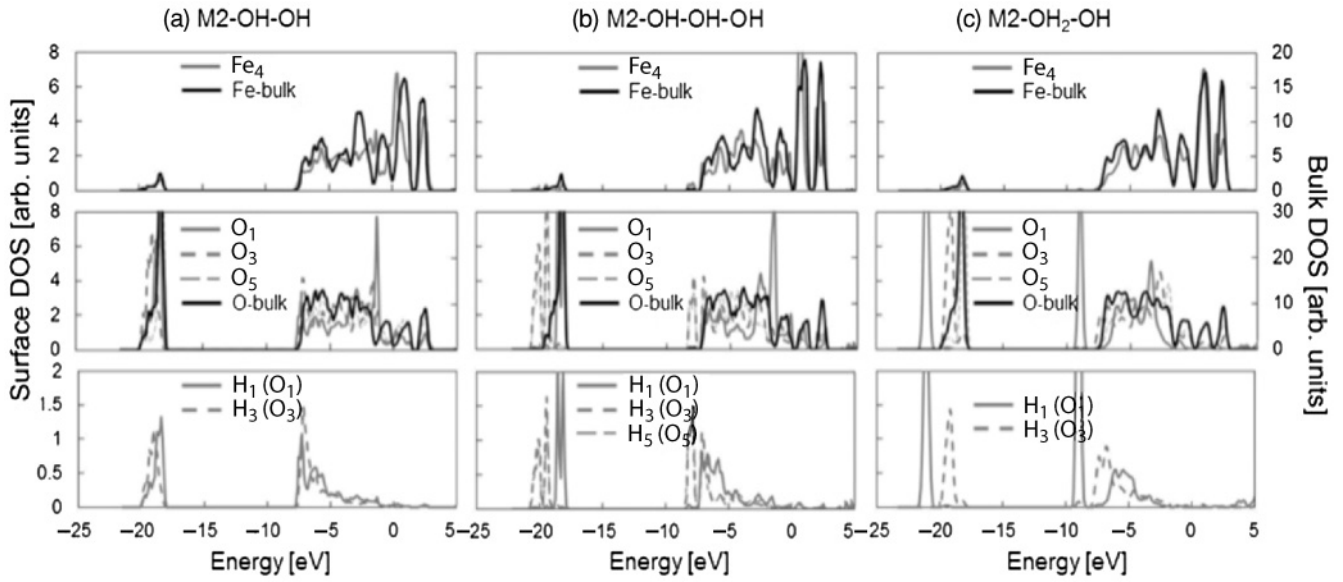

FIG. 6. DOS for the most stable hydroxylated M2 surfaces of α-Fe_2O_3, for (a) M2-OH-OH, (b) M2-OH-OH-OH, and (c) M2-OH_2-OH.

Electronic structure calculations were used to characterize the Lewis acid-base sites on the various M2 α-Al_2O_3 and α-Fe_2O_3 r-cut surfaces. The acidity of the surface is due primarily to the cations, which act as electron-acceptor sites. Figures 5 and 6 show plots of the DOS for the three most stable M2 surfaces of α-Al_2O_3 and α-Fe_2O_3, respectively, where the Fermi level is defined at 0 eV. Comparison of the DOS of the three hydroxylated M2 α-Al_2O_3 surfaces (Fig. 5) shows that the (a) M2-OH-OH surface has the weakest Lewis acid sites, with empty cation sites at the highest energy of approximately 5.2 eV above the Fermi level. In comparison, the lowest acceptor sites for the (b) M2-OH-OH-OH and (c) M2-OH_2-OH surfaces occur at lower energies, approximately 4.5 and 5 eV above the Fermi level, respectively. In the case of the M2-OH-OH-OH surface of α-Al_2O_3, which best matches the experimental structural data, the bulk states are lower in energy compared to the Fermi level. The clear overlap of the electronic states of the top-layer Al cations and the top-layer oxygen atoms signifies a strong interaction between these atoms, and the close proximity to the Fermi level suggests stronger Lewis base character. In addition, comparison of the hydrogen atom DOS in Figs. 5(b) and 5(c) shows that the main surface hydrogen peaks are much lower in energy for the M2-OH_2-OH surface and the hydrogen atoms should, therefore, be more tightly bound.

Comparison of the DOS of α-Fe_2O_3 (Fig. 6) with the DOS of α-Al_2O_3 shows a much higher concentration of electron-acceptor sites from the *d* states of the Fe atoms within the band gap compared with the *p* states of the Al atoms. In fact, a clear band gap is no longer present for the α-Fe_2O_3 surfaces. This loss of a band gap also is observed for the bulk anion and cation states because the bulk atoms still undergo some surface relaxation and are not completely equivalent to the true bulk atom arrangement. It is not clear how this result influences the overall DFT-computed surface reactivity, and there is debate about whether using the DFT + U approach for investigating the surface will improve the quality of the results.[33] Nonetheless, it is clear that the number of empty Fe states at the α-Fe_2O_3 r-cut surface is very high and close to the Fermi level and will contribute to a much stronger degree of reactivity in terms of its Lewis acid sites compared to the α-Al_2O_3 r-cut surface. For all of the hydroxylated M2 surfaces considered, the overall electron distribution of the hydrogen and oxygen atoms is much farther from the Fermi level for α-Fe_2O_3 relative to α-Al_2O_3, indicating that the bonding interactions are more stable; however, there are also

TABLE IV. Band gap (E_g), work function (ϕ_{wf}), and change in charge of the surface cations (ΔQ_M), oxygen atoms (ΔQ_O), and hydrogen atoms (ΔQ_H) for the most stable hydroxylated M2 r-cut surfaces of α-Al_2O_3 and α-Fe_2O_3. The specific atom is denoted in parentheses.

Structure	E_g (eV)	ϕ_{wf} (eV)	ΔQ_M (e)	ΔQ_O (e)	ΔQ_H (e)
Al_2O_3 M2-OH-OH	4.68	7.32	−0.03 (Al_4)	0.03 (O_1) 0.47 (O_3)	0.03 (H-O_1) 0.50 (H-O_3)
Al_2O_3 M2-OH-OH-OH	3.48	6.24	−0.02 (Al_4)	−0.17 (O_1) 0.44 (O_3) 0.14 (O_5)	0.06 (H-O_1) 0.60 (H-O_3) 0.33 (H-O_5)
Al_2O_3 M2-OH_2-OH	3.15	4.60	−0.01 (Al_4)	−0.03 (O_1) 0.11 (O_3)	0.37/0.15 (H-O_1) 0.26 (H-O_3)
Fe_2O_3 M2-OH-OH		5.95	−0.04 (Fe_4)	−0.46 (O_1) 0.05 (O_3)	0.04 (H-O_1) 0.41 (H-O_3)
Fe_2O_3 M2-OH-OH-OH		5.73	0.05 (Fe_4)	−0.49 (O_1) 0.12 (O_3) 0.17(O_5)	0.06 (H-O_1) 0.66 (H-O_3) 0.32 (H-O_5)
Fe_2O_3 M2-OH_2-OH		5.21	0.00 (Fe_4)	−0.60 (O_1)-0.26 (O_3)	0.37/0.12 (H-O_1) 0.22 (H-O_3)

more empty states near the Fermi level that are more readily available to participate in surface interactions.

Although the Lewis acid strength of the surface can be determined by the location of the empty electronic states of the cations (or protons), the highest occupied orbitals of the surface oxygen atoms are typically correlated with the Lewis basicity of the surface. Unfortunately, these filled states are less localized, and it is more difficult to determine the relative strength of the basic sites using only DOS information. Instead, it is possible to measure and to compare the work functions of the various surfaces, which will tend to decrease for stronger Lewis base sites. Here, we define the work function as the difference between the Fermi energy and the energy in the vacuum region of the computational domain, which is a reasonable measure of the minimum energy necessary to remove an electron from the oxide surface. Table IV gives the work function, band gap, and change in electron charge for the three most stable hydroxylated M2 α-Al_2O_3 and α-Fe_2O_3 r-cut surfaces. It is well known that DFT generally underestimates the band gaps in metal oxides, and this problem is observed in this paper as well. However, in our analysis, we are mainly concerned with the changes in the band gap, which should be unaffected by the smaller calculated band gap.

Because the electronegativities of the four types of atoms in these surfaces are significantly different [Fe (1.83), Al (1.61), O (3.44), and H (2.20)],[34] it is useful to examine the change in charge of the surface atoms as a function of metal atom type and hydroxylation. The value of the calculated Bader charge of the individual bulk Fe and O atoms in α-Fe_2O_3 are $1.40e$ and $-0.93e$, respectively, whereas, they are $2.32e$ and $-1.54e$, respectively, for bulk Al and O in α-Al_2O_3, which is consistent with the differences in the electronegativities of these atoms. In other words, since the relative difference in electronegativity is larger between Al and O compared with Fe and O, the oxygen atoms in α-Al_2O_3 will gain more electron density from the cations than the oxygen atoms in α-Fe_2O_3. The change in charge shown in Table IV was calculated by subtracting the Bader charge of (1) the bulk oxygen atoms from the hydroxylated oxygen atoms, (2) the bulk cations from the surface cations, and (3) one from the hydrogen atoms. A positive change means that there is an overall loss in the number of electrons and, therefore, a more positive charge on the surface atom compared with the bulk atom charge. In all cases, the hydrogen atoms lose electron density. The top oxygen atoms of the M2-OH-OH-OH surface acquire the most charge compared with the bulk of each of the hydroxylated α-Al_2O_3 surfaces considered here, with an increase in electron charge of $-0.17e$. This result suggests that this top O_1 site will act as a strong Lewis base. Although the trends are similar for both the hydrated α-Al_2O_3 and the α-Fe_2O_3 r-cut surfaces, where the highest and lowest work functions correspond to the M2-OH_2-OH and M2-OH-OH surfaces, respectively, the range of work function values is much different. For example, the calculated work functions of the three r-cut surfaces of α-Fe_2O_3 are relatively similar, ranging between 5.21 and 5.95 eV. In comparison, the work functions of the α-Al_2O_3 r-cut surfaces show much more variability. In fact, the work function of the M2-OH_2-OH surface for α-Al_2O_3 is less than any of the work functions calculated for α-Fe_2O_3, suggesting that this surface is the more reactive in terms of its Lewis basicity. On the other hand, the α-Al_2O_3 M2-OH_2-OH and M2-OH-OH-OH surfaces have much higher work functions compared to the α-Fe_2O_3 r-cut surfaces and, therefore, have much weaker basic character.

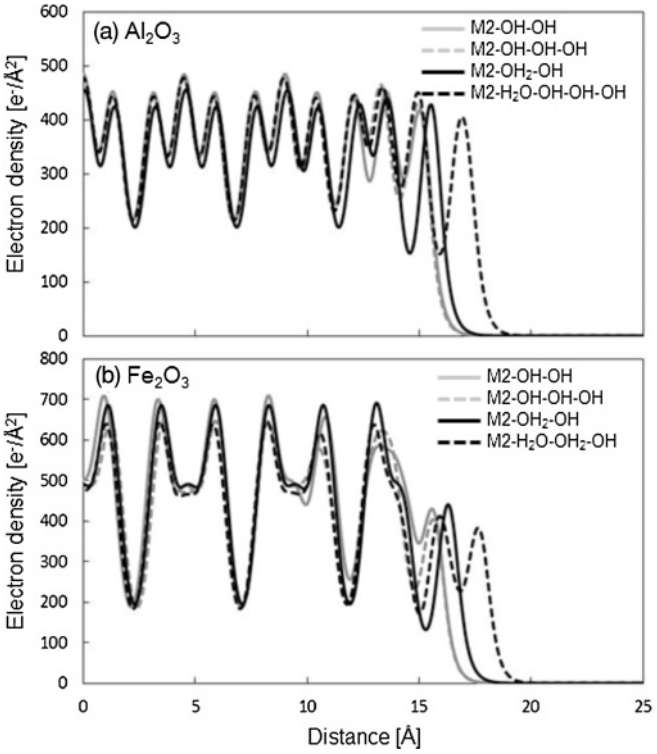

FIG. 7. Average electron density along the direction perpendicular to the surface of (a) α-Al_2O_3 and (b) α-Fe_2O_3 for the most thermodynamically stable hydroxylated r-cut surface and the surface with on monolayer of water with a geometric structure that matches best with experimental CTR x-ray diffraction measurements.

Figure 7 shows a plot of the electron density averaged along the direction perpendicular to the r-cut surface for the three M2 surfaces of (a) α-Al_2O_3 and (b) α-Fe_2O_3. Each structure is characterized by a periodic array of three peaks, although in the case of α-Fe_2O_3, the center peak is very small, and for α-Al_2O_3, the center peak is the highest one. The α-Fe_2O_3 electron-density plot is much closer to the results of high-resolution specular x-ray reflection measurements.[10] Another significant difference between the two types of oxides is the electron density at the surface. In α-Al_2O_3, the surface oxygen atoms and hydroxyl groups do a much better job mimicking the charge distribution in the bulk as compared to the α-Fe_2O_3 surfaces. Also, the addition of a layer of water changes the charge distribution of the α-Fe_2O_3 surface more than the α-Al_2O_3 surface. All three of the hydroxylated M2 surfaces of α-Al_2O_3 have essentially the same electron density at the surface, although in the case of the M2-OH_2-OH surface, there appears to be a much stronger dipole. This dipole layer and not the overall charge may be what generates the smaller work function at this surface and, therefore, the greater strength of the Lewis base sites. Specular x-ray reflectivity studies[10] have shown that ordering of water decays much faster away from the oxide-water interface in α-Fe_2O_3 than in α-Al_2O_3,

TABLE V. Calculated BVs of the first six atomic layers in the most stable hydroxylated M2 r-cut surfaces of α-Al_2O_3 and α-Fe_2O_3. The labels refer to (a) BV due only to coordination by the cation, (b) BV including that due to hydroxylation of the oxygen, and (c) BV with all contributions, including those from the hydrogen-bonding network.

Layer	α-Al_2O_3 M2-OH-OH (v.u.)	α-Al_2O_3 M2-OH-OH-OH (v.u.)	α-Al_2O_3 M2-OH_2-OH (v.u.)	α-Fe_2O_3 M2-OH-OH (v.u.)	α-Fe_2O_3 M2-OH-OH-OH (v.u.)	α-Fe_2O_3 M2-OH_2-OH (v.u.)
O_1	0.59 (a) 1.52(b) 2.06 (c)	0.73 (a) 1.70(b) 2.33 (c)	0.23 (a) 2.10(b) 2.29 (c)	0.76 (a) 1.70(b) 2.24 (c)	0.68 (a) 1.63(b) 2.22 (c)	0.26 (a) 2.05(b) 2.24 (c)
O_3	1.07 (a) 2.01(b) 2.38 (c)	1.06 (a) 2.02(b) 2.71 (c)	0.94 (a) 1.79(b) 2.39 (c)	1.10 (a) 2.00(b) 2.38 (c)	0.94 (a) 1.93(b) 2.47 (c)	0.85 (a) 1.76(b) 2.34 (c)
Al_4/Fe_4	3.19	3.08	2.91	3.79	3.09	2.77
O_5	1.75 (a) 2.13 (c)	1.47 (a) 2.25 (b) 2.61 (c)	1.71 (a) 2.22 (c)	2.05 (a) 2.43 (c)	1.34 (a) 2.16 (b) 2.41 (c)	1.75 (a) 2.22 (c)
O_6	1.97	1.86	2.05	1.99	1.97	1.97
Al_7/Fe_7	3.16	3.12	3.10	3.18	3.05	2.97

which could be the result of the greater reduction in the electron density of the α-Fe_2O_3 surfaces at the interface.

To further understand the role of the protons in the reactivity of the hydroxylated oxygen atoms, BV can be used to probe the strength of the Brønsted acidity of the surface hydroxyl groups by providing a measure of the relative coordination of the surface oxygen atoms and the metal cations. The BVs of the most stable M2 surfaces for α-Al_2O_3 and α-Fe_2O_3 are given in Table V. The BVs of the oxygen atoms are divided into three components corresponding to (a) BV due only to coordination by the cation, (b) BV including that due to hydroxylation of the oxygen (typical OH internal distance is on the order of 1 Å), and (c) BV with all contributions, including those from the hydrogen-bonding network (typical hydrogen-bonding distances are on the order of 2.5–3 Å). The overall reactivity of the hydroxyl groups should depend primarily on the BV contributed from the directly bonded ions with smaller contributions from the hydrogen-bonding network. Excluding the contribution from hydrogen bonding, the BVs of the surface hydroxyl groups of all the surfaces considered agree reasonably well with the atomic valences.[35] The contribution from the hydrogen-bonding network results in overbonding of the hydroxide ions, making the configuration less stable and increasing their Brønsted acid strengths. Comparison of the BV values of the α-Al_2O_3 r-cut surfaces shows that the least stable one is the M2-OH_2-OH surface, which has a BV of 2.10 v.u. (2.29 v.u. including all hydrogen bonding) for the top hydroxide ions. The higher reactivity at this site is consistent with electronic calculations discussed in Sec. III C, which also predict this surface of corundum to be the most reactive. In comparison, all three α-Fe_2O_3 r-cut surfaces have more similar BVs including those with contributions from the hydrogen-bonding network; however, the BV of the top hydroxyl group is still highest for the M2-OH_2-OH surface when the indirect hydrogen bonds are not included. It is interesting to note that, in almost all cases, the BVs of the second- and third-layer hydroxyl groups are higher than the topmost hydroxyl group.

E. Magnetic moments of α-Fe_2O_3 surface atoms

The magnetic moments of the surface Fe atoms were calculated for the M2-OH-OH, M2-OH_2-OH, and M2-OH-OH-OH α-Fe_2O_3 r-cut surfaces. Although hematite is antiferromagnetic, the magnetic moment of each individual Fe atom is $\pm 3.50 \mu_B$ in the bulk, which is reasonably consistent with the experimental value ($4.6 - 4.9 \mu_B$).[25] The spin states of all of the atoms are maintained in the same configuration as dictated by the antiferromagnetic ordering of the bulk. The magnetic moment of the Fe atoms increases to $\pm 3.70 \mu_B$ and $\pm 3.62 \mu_B$ for the M2-OH-OH-OH and M2-OH_2-OH surfaces, respectively, and decreases to $\pm 2.08 \mu_B$ for the M2-OH-OH surface. This trend is consistent with the calculated Bader charges for the Fe atoms, which increase to $1.48e$ and $1.41e$ for the first two surfaces and decrease to $1.36e$ for the third surface. A complete set of simulations to investigate the influence of spin canting (i.e., when the spins are deflected or canted away from the antiferromagnetic plane) of the surface cations was not undertaken in this paper, but to understand how spin ordering on the surface might impact the stability, simulations were run with the surface spin states aligned. Without allowing the atomic coordinates of the surfaces to relax in response to the different spin configurations, the free energy of the surfaces increased by 0.37, 1.10, and 1.75 eV for the M2-OH-OH, M2-OH-OH-OH, and M2-OH_2-OH surfaces, respectively. In

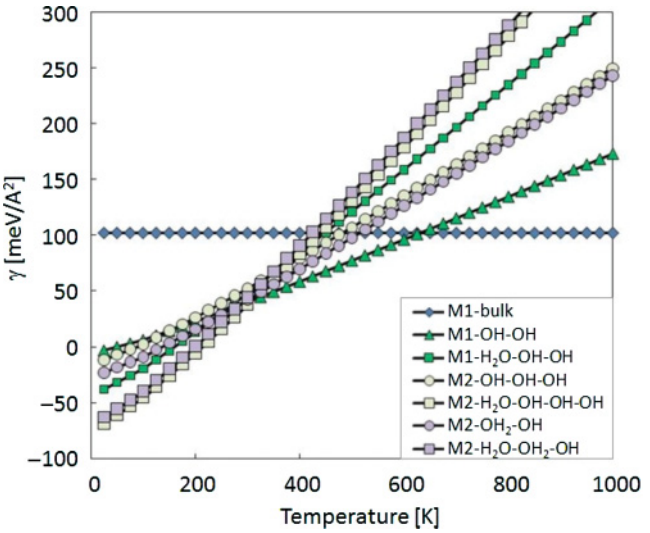

FIG. 8. (Color online) Surface free energy as a function of temperature for $pO_2 = 10^{-8}$ Torr and $pH_2O = 1.6$ Torr of the most energetically stable hydrated α-Al_2O_3 r-cut surface structures.

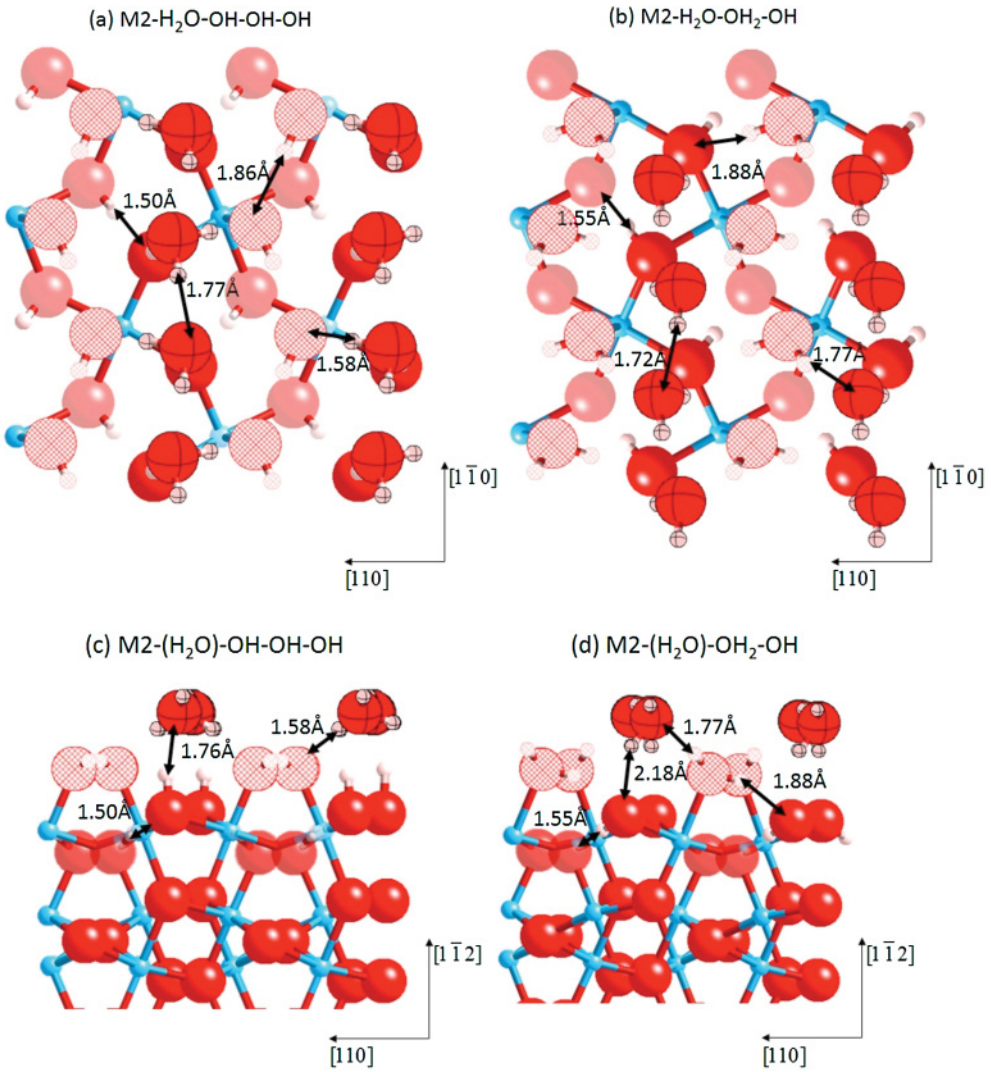

FIG. 9. (Color online) The two most energetically stable low temperature $[1\,\bar{1}02]\alpha$-Al_2O_3 surface configurations corresponding to the top view of (a) M2-H_2O-OH-OH-OH and (b) M2-H_2O-OH_2-OH and the side view of (c) M2-H_2O-OH-OH-OH and (d) M2-H_2O-OH_2-OH. Arrows denote distances between the oxygen atoms and the nearest nonbonded hydrogen atoms. The hatched atoms denote the oxygen atoms terminating the surface.

addition to the changes in spin magnetic moment of the surface Fe atoms compared to the bulk, the top surface oxygen atoms of the M2-OH-OH-OH surface acquired a spin magnetic moment of $\pm 0.25\mu_B$. In comparison, the magnetic moments of the other oxygen atoms in the M2-OH-OH-OH surface and all the oxygen atoms in all other surfaces considered were found to be essentially zero (lower than $0.07\mu_B$).

F. Hydrated α-Al_2O_3 r-cut surfaces

CTR diffraction experiments showed that dosing the α-Al_2O_3 r-cut surface with water did not change its geometric structure,[14] which led to the conclusion that the surface was already saturated with water. In this paper, the effect of physisorbed water on the alumina surface was investigated by adding one, two, and three layers of water molecules to the most thermodynamically stable hydroxylated r-cut surfaces of α-Al_2O_3. The stabilities of these surfaces as a function of temperature are shown in Fig. 8. The inclusion of a single monolayer of water reduced the surface free energy of the M2-OH-OH-OH and M2-OH_2-OH surfaces by approximately 55 and 40 meV/Å^2, respectively, which makes the former surface the more thermodynamically stable one.

Shown in Fig. 9 are structures of the (a) and (c) M2-H_2O-OH-OH-OH and (b) and (d) M2-H_2O-OH_2-OH surfaces with the distances given between the oxygen atoms and the nearest nonbonded hydrogen atoms. Examination of the two structures side by side reveals similarities in the hydrogen-bonding network. In both cases, a hydrogen atom is shared between second-layer (O_3) and third-layer (O_5) oxygen atoms, which are both bound to the first-layer Al (Al_4) atoms. In the M2-OH-OH-OH surface, the hydrogen atom is bound to O_5 and is 1.50 Å away from O_3, whereas, the hydrogen atom in the M2-OH_2-OH surface is bound to O_3 and is 1.54 Å away from O_5. Furthermore, the hydrogen atom attached to O_3 [Fig. 9(c)] is in a very similar position to the hydrogen atom attached to the water molecule that is oriented toward the surface in Fig. 9(d) and likewise for the hydrogen atom

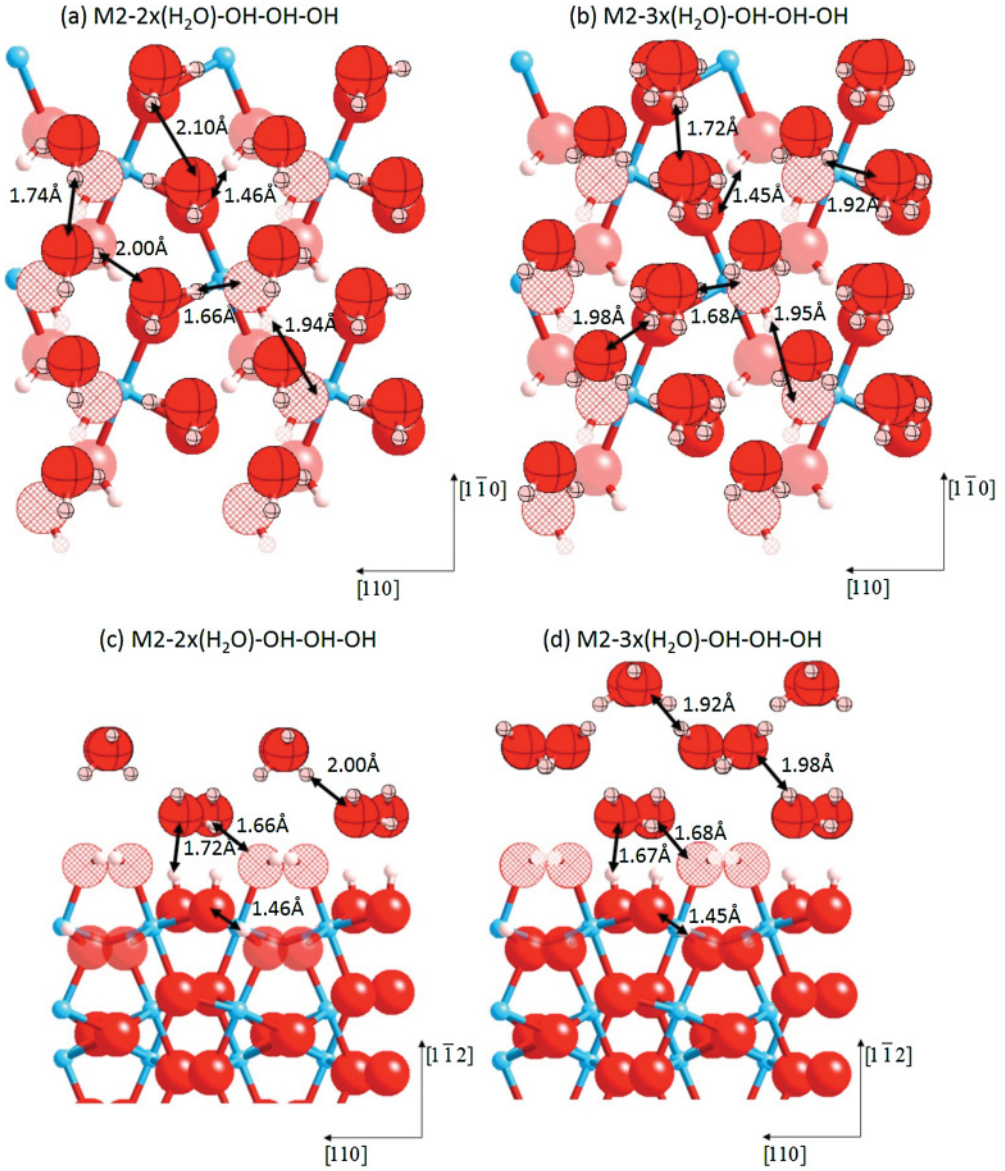

FIG. 10. (Color online) The α-Al_2O_3 M2-OH-OH-OH surface with two (M2-2×H_2O-OH-OH-OH) and three (M2-3×H_2O-OH-OH-OH) layers of water (a), (b) top view and (c), (d) side view. Arrows denote distance between hydrogen atoms and nearest nonbonded neighboring oxygen atoms. The hatched atoms denote the oxygen atoms terminating the surface.

attached to the water molecule in Fig. 9(c) at a distance of 1.58 Å from O_3 and the second hydrogen atom attached to O_3 in Fig. 9(d). Considering that the surface free-energy difference of these two structures is very small, one surface could easily transform into the other. Given the higher reactivity of the α-Al_2O_3 M2-OH_2-OH surface, it is probable that this surface represents a higher-energy structure that will transition to the M2-OH-OH-OH surface. Further work using nudged elastic band calculations will be undertaken to determine the activation barrier between these two surface configurations and to investigate the kinetic limitations between potential transformations between these two hydrated M2 surfaces.

Table VI reports the change in layer spacing of the most stable M2 r-cut surfaces hydrated with a single monolayer of water. The addition of a monolayer of water changes the layer spacing of the α-Al_2O_3 M2-H_2O-OH_2-OH r-cut surface in a way that is consistent with the layer relaxation of the analogous α-Fe_2O_3 M2-H_2O-OH_2-OH r-cut surface observed by Lo *et al.*,[13] although in contrast with those results in the case of α-Al_2O_3, the relaxation does not lead to better agreement with the CTR diffraction data. In comparison, the layer spacing of the M2-OH-OH-OH surface does not change significantly with the addition of water (Table VI), and this spacing still has the best overall agreement with the CTR diffraction results. Furthermore, simulations were also carried out with two and three layers of water molecules physisorbed on the α-Al_2O_3 M2-OH-OH-OH surface. At 0 K, the surface free energy is further reduced by approximately 30 meV/Å for each additional monolayer of water, but the presence of the extra water molecules does not result in a significant change in the layer relaxation except for the very topmost surface oxygen atoms. The addition of a single layer of water molecules

TABLE VI. Atomic layer relaxation of the two most stable hydrated M2 r-cut surfaces for α-Al_2O_3. The percent relaxation compared to the bulk is shown in parentheses.

Layer	M2-H_2O-OH_2-OH (Å)	M2-H_2O-OH-OH-OH (Å)
$\Delta(H_2O\text{-}O_1)$	1.575	1.520
$\Delta(O_1\text{-}O_3)$	1.279 (18.7%)	1.176 (9.2%)
Δ (O_3-Al_4)	0.663 (−7.6%)	0.489 (−31.8%)
Δ (Al_4-O_5)	0.411 (14.1%)	0.579 (61.8%)
Δ (O_5-O_6)	1.334 (−1.9%)	1.262 (−7.2%)
Δ (O_6-Al_7)	0.387 (7.6%)	0.438 (22.5%)
Δ (Al_7-O_8)	0.726 (1.3%)	0.677 (−5.6%)
Δ (O_8-Al_9)	0.707 (−1.4%)	0.678 (−5.5%)
Δ (Al_9-O_{10})	0.358 (−0.7%)	0.373 (4.4%)

decreased the relaxation from 15.9% to 9.2%, whereas, the relaxation increased to 15.0% and to 16.4%, respectively, when two and three layers of water molecules were included. Additional water layers on the surface could act to further increase the percent relaxation, but it does not seem likely that the interactions of these additional physisorbed water layers will be strong enough to reproduce the 32.9% relaxation measured experimentally.

Figure 10 shows a plot of the atomic structure of the M2-OH-OH-OH surface with two and three layers of physisorbed water. An exhaustive investigation of all possible orientations of water molecules on the hydrated α-Al_2O_3 and α-Fe_2O_3 r-cut surfaces is not possible with the DFT simulations due to time and computational limitations. The initial positions of water molecules where chosen based on the converged structure of the single water layer structure in terms of both the position of the oxygen atoms and the hydrogen-bonding network. While not comprehensive, the final converged structures can be used to understand the general trends in how water influences these surfaces. It would be interesting to calculate the resulting electron localization function of these surfaces both to ensure that the most important hydrogen-bonded interactions were accounted for and to investigate the surface reactivity.[36]

Besides changing the layer spacing of the top hydroxyl groups slightly (∼0.1 Å), increasing the number of water layers also impacts the lateral position of the adsorbed water molecules. The topmost layer of water molecules is more dispersed along the [110] direction. Although simulations of all possible configurations of ordered water on the surface have not been investigated, the addition of two and three layers of water does not significantly change the layer relaxation of the α-Al_2O_3 surface structure as shown in Fig. 11, which provides a graphical comparison of the percent relaxation for the different simulated configurations.

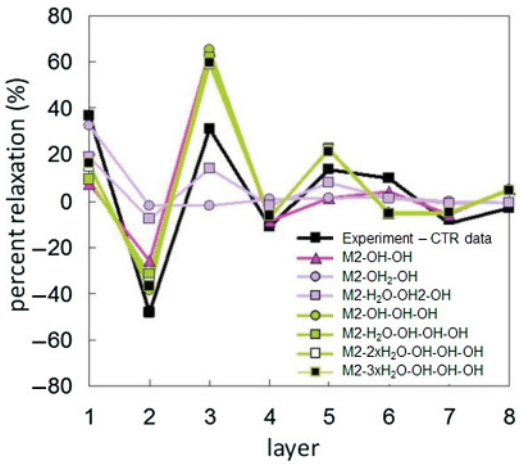

FIG. 11. (Color online) The percent layer relaxation for the most stable M2 hydroxylated and hydrated r-cut surfaces of α-Al_2O_3.

G. Role of water in the surface reactivity of α-Al_2O_3

The BVs calculated for each of the top six O and Al atoms of the two energetically stable M2 hydrated structures, M2-H_2O-OH-OH-OH and M2-H_2O-OH_2-OH are reported in Table VII. Again, there are three different types of contributions to the BV sum of the oxygen atoms: (a) the BV due only to coordination by cations, (b) the BV including hydroxylation of the oxygen atoms, and (c) the BV with all contributions, including the contribution from hydrogen bonding. The trends in the BV values for the hydroxylated oxygen species in the two surfaces are very different and signify a difference in reactivity of the bihydroxylated surface vs the three-layer monohydroxylated surface. The top bihydroxylated hydroxyl group represents the strongest Brønsted acid species for the nonhydrated M2-OH_2-OH surface, with an oxygen (O_1) BV of 2.29 v.u. compared with 2.11 v.u. for the second hydroxylated oxygen atom (O_3). The inclusion of a monolayer of water, which has a high oxygen BV of 2.25 v.u., increases the BV of O_1 to 2.87 and that of O_3 to 2.33 v.u. Neglecting the contribution to the BV from all the hydrogen atoms, the third-layer oxygen atom (O_5) has a relatively low BV of 1.65 v.u. In comparison, the top hydroxyl group of the water-covered monohydroxylated M2-OH-OH-OH surface is much less reactive than the bihydroxylated one with a BV of O_1 of 2.37 v.u. The second- and third-layer oxygen atoms, O_3 and O_5, also have comparable BV values of 2.25 and 2.33, respectively. The BV trends of the O_1, O_3, and O_5 oxygen atoms in the bihydroxylated and monohydroxylated surfaces clearly support the proposed transformation pathway between these two surfaces.

The strong Brønsted acidity of O_1 and O_3 on the water-covered bihydroxylated surface could drive the hydrogen

TABLE VII. Calculated BVs of the first six atomic layers in the two most stable hydrated M2 r-cut surfaces of α-Al_2O_3. The labels refer to (a) BV due only to coordination by the cation, (b) BV including that due to hydroxylation of the oxygen, and (c) BV with all contributions, including those from the hydrogen-bonding network.

Atom	M2-H_2O-OH_2-OH (v.u.)	M2-H_2O-OH-OH-OH (v.u.)
H_2O	1.88 (b) 2.56 (c)	1.78 (b) 2.25 (c)
O_1	0.32 (a) 2.17 (b) 2.87 (c)	0.69 (a) 1.63 (b) 2.37 (c)
O_3	0.90 (a) 1.70 (b) 2.33 (c)	1.06 (a) 1.70 (b) 2.25 (c)
Al_4	2.83	3.02
O_5	1.65 (a) 2.05 (c)	1.43 (a) 2.20 (b) 2.33 (c)
O_6	1.96	1.87
Al_7	3.05	3.11

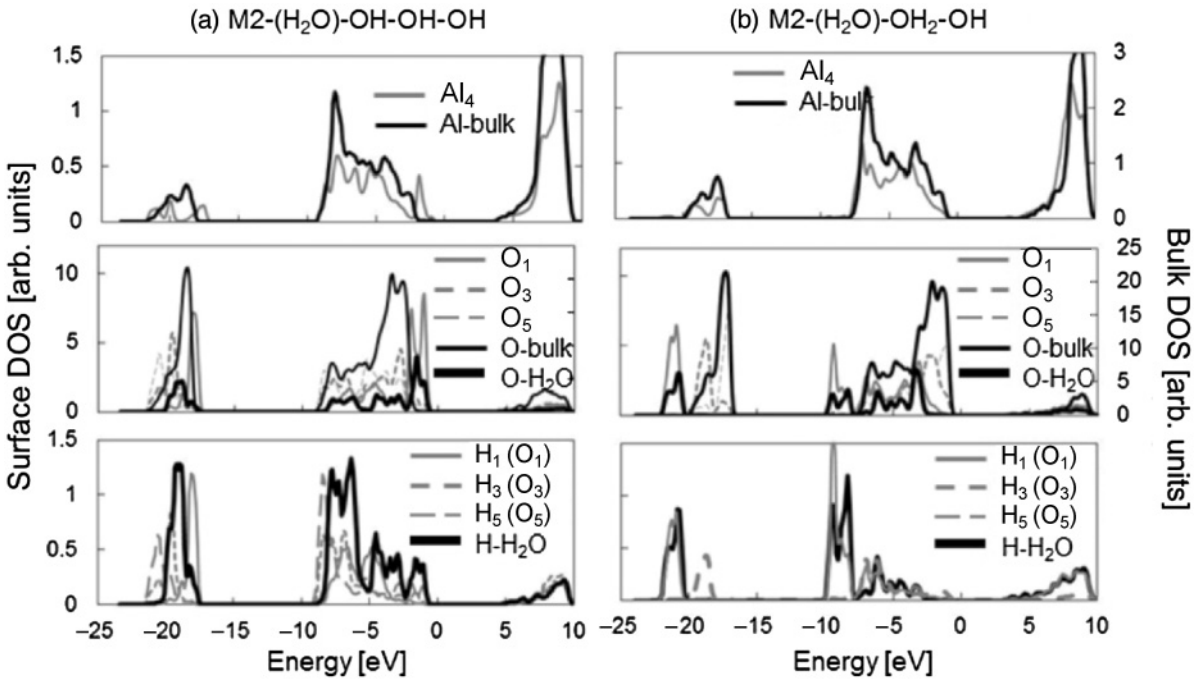

FIG. 12. DOS for the two stable hydrated M2 surfaces of α-Al_2O_3, where (a) is the M2-(H_2O)-OH-OH-OH surface and (b) is the M2-(H_2O)-OH_2-OH surface.

atoms deeper into the bulk, resulting in hydroxylation of O_5 and leaving O_1 singly hydroxylated. The inclusion of the extra hydrogen atoms in the bulk would then act to change the atomic layer spacing as the atoms readjust and reduce the BV. The resulting hydroxylated oxygen atoms in this monohydroxylated surface (M2-OH-OH-OH) are still slightly acidic in nature as seen from the BV but less so than those in the bihydroxylated surface (M2-OH_2-OH). This observation suggests that once formed, the hydrogen atoms in the M2-OH-OH-OH configuration are more likely to remain in this state, which has the atomic spacing that best matches the CTR diffraction results. It is also interesting to note that the hydrated M2-OH_2-OH surface was exceedingly sensitive to the initial configuration guess, and it was very difficult to obtain energy convergence compared with the other structures, including the hydrated M2-OH-OH-OH surface. This difficulty may be reflective of a potential-energy barrier toward forming this structure and could indicate that this configuration is more likely to be an initial state. If the hydrated M2-OH_2-OH represents a local minimum of the potential-energy landscape (as compared to a global minimum) that is very shallow, then it might be difficult to obtain convergence to this state, which is what we find.

The oxygen BV of the physisorbed water species is significantly larger for three water layers compared to two water layers on the M2-OH-OH-OH r-cut surface as shown in Table VII. The high Brønsted acidity arises from the hydrogen-bonding network between neighboring water molecules and the hydroxylated oxygen atoms on the surface. Given the high oxygen BV, these physisorbed water molecules should reorient themselves to reduce their interaction with neighboring hydrogen atoms. The influence of the hydrogen-bonding network is not as high for the monohydroxylated structure with one or two layers of physisorbed water, and the oxygen BV is appreciably lower. High-resolution specular x-ray reflectivity experiments by Catalano *et al.*[10] found that only two layers of water molecules are physisorbed on the r-cut surface of α-Al_2O_3. Additional water molecules should be in a layered bulklike structure that decays in its degree of ordering with distance from the surface. The high oxygen BV values found in the third water layer may play a role in reducing the structural order of the physisorbed water.

The DOS of the surface layer of hydrogen atoms on the α-Al_2O_3 r-cut surface is much more diffuse when water is present (Fig. 12), which signifies the influence of the hydrogen-bonding network between the water and the surface oxygen atoms. The overlap in the hydrogen and oxygen DOS at approximately -22 and -9 eV shows an interaction between the surface hydrogen atoms and the hydrogen atoms in the physisorbed water layer, which contributes to the decrease in the bond strength between the two hydrogen atoms bonded to O_1.

IV. CONCLUSIONS

Without the inclusion of physisorbed water layers on the metal oxide surfaces, the *ab initio* thermodynamics calculations predict the M2-OH_2-OH r-cut surface to be the most energetically stable one for both α-Al_2O_3 and α-Fe_2O_3, although neither of these structures match the results of CTR diffraction experiments. In the case of α-Al_2O_3, the best structural match between the experiments and the DFT calculations is for the M2-OH-OH-OH surface. Interestingly, when physisorbed water was included in the simulations, the layer spacing of the M2-OH-OH-OH α-Al_2O_3 surface did not

change appreciably, although the energetic stability relative to the M2-OH_2-OH surface increased. This is in contrast to previous DFT studies which found that the inclusion of a monolayer of water on the M2-OH_2-OH surface of α-Fe_2O_3 is necessary to give good agreement with experiment. In other words, the α-Fe_2O_3 surface is found to be much more sensitive to the presence of physisorbed water molecules than the α-Al_2O_3 surface. The configuration of hydroxyl groups of the most stable surface structures predicted with DFT is also different for α-Al_2O_3 and α-Fe_2O_3. The protons penetrate much deeper into the bulk material for α-Al_2O_3 with three layers of hydroxyl groups compared to only two layers for α-Fe_2O_3.

Differences in reactivity of the α-Al_2O_3 and α-Fe_2O_3 r-cut surfaces were investigated by comparing the DOS and BVs for the different surfaces. Overall, the higher reactivity of the r-cut surface of α-Fe_2O_3 can be attributed mainly to the empty *d* states of the surface Fe atoms, which result in very strong Lewis acid sites that are clearly shown in the DOS as acceptor sites very close to the Fermi level with a maximum peak at less than 1 eV above. In comparison, the empty *p* states of Al are on the order of 5 eV above the Fermi level and should be much less reactive to potential adsorbates. Furthermore, the calculated electron distribution for the α-Al_2O_3 r-cut surface is more consistent with the bulklike structure of α-Al_2O_3, whereas, the structure of the α-Fe_2O_3 r-cut surface is more relaxed compared to the bulk α-Fe_2O_3. This increased relaxation is also predicted when an additional monolayer of physisorbed water is added to the α-Fe_2O_3 bihydroxylated r-cut surface, which could help explain why water ordering is found to extend farther away from the r-cut α-Al_2O_3/water interface compared to α-Fe_2O_3.

ACKNOWLEDGMENTS

This research was supported by the Stanford Environmental Molecular Science Institute (EMSI) (NSF Grant No. CHE-0431425) and, in part, by the National Science Foundation through TeraGrid resources provided by the Texas Advanced Computing Center (TACC). Additional computational resources were provided by the Stanford Center for Computational Earth and Environmental Science (CEES).

*Shela.Aboud@stanford.edu

[1] T. P. Trainor, A. S. Templeton, and P. J. Eng, J. Elec. Spectros. Rel. Phenom. **150**, 66 (2006).

[2] G. E. Brown Jr., T. P. Trainor, and A. M. Chaka, in *Chemical Bonding at Surfaces and Interfaces*, edited by A. Nilsson, L. G. M. Pettersson, J. K. Nørskov (Elsevier, Amsterdam, 2008), pp. 457–509.

[3] T. P. Trainor, A. M. Chaka, P. J. Eng, M. Newville, G. A. Waychunas, J. G. Catalano, and G. E. Brown Jr., Surf. Sci. **573**, 204 (2004).

[4] P. J. Eng, T. P. Trainor, G. E. Brown Jr., G. A. Waychunas, M. Newville, S. R. Sutton, and M. L. Rivers, Science **288**, 1029 (2000).

[5] J. G. Catalano, T. P. Trainor, P. J. Eng, G. A. Waychunas, and G. E. Brown Jr., Geochim. Cosmochim. Acta **69**, 3555 (2005).

[6] J. R. Barger, S. N. Towle, G. E. Brown Jr., and G. A. Parks, Geochim. Cosmochim. Acta **60**, 3541 (1996); J. Colloid Interface Sci. **185**, 473 (1997); A. S. Templeton, T. P. Trainor, S. J. Traina, A. M. Spormann, and G. E. Brown Jr., Proc. Natl. Acad. Sci. USA **98**, 11897 (2001); T. P. Trainor, A. S. Templeton, G. E. Brown Jr., and G. A. Parks, Langmuir **18**, 5782 (2002); J. R. Barger, T. P. Trainor, J. P. Fitts, S. A. Chambers, and G. E. Brown Jr., Langmuir **20**, 1667 (2004).

[7] S. E. Mason, C. R. Iceman, K. S. Tanwar, T. P. Trainor, and A. M. Chaka, J. Phys. Chem. C **113**, 2159 (2009); G. E. Brown Jr., Science **294**, 69 (2001).

[8] P. Liu, T. Kendelewicz, G. E. Brown Jr., E. J. Nelson, and S. A. Chambers, Surf. Sci. **417**, 53 (1998).

[9] J. O'M. Bockris and K. T. Jeng, Adv. Colloid Interface Sci. **33**, 1 (1990); J. O'M. Bockris and S. U. M. Khan, *Surface Electrochemistry. A Molecular Level Approach* (Plenum, New York 1993); D. A. Sverjensky, Geochim. Cosmochim. Acta **65**, 3643 (2001).

[10] J. G. Catalano, C. Park, Z. Zhang, and P. Fenter, Langmuir **22**, 4668 (2006); J. G. Catalano, P. Fenter, and C. Park, Geochim. Cosmochim. Acta **71**, 5313 (2007).

[11] J. G. Catalano, C. Park, P. Fenter, and Z. Zhang, Geochim. Cosmochim. Acta **72**, 1986 (2008).

[12] L. Pauling, *The Nature of the Chemical Bond* (Cornell University Press, Ithaca, NY, 1960).

[13] C. S. Lo, K. S. Tanwar, A. M. Chaka, and T. P. Trainor, Phys. Rev. B **75**, 075425 (2007).

[14] T. P. Trainor, P. Eng, G. E. Brown Jr., I. K. Robinson, and M. De Santis, Surf. Sci. **496**, 238 (2002).

[15] K. S. Tanwar, C. S. Lo, P. J. Eng, J. G. Catalano, D. K. Walko, G. E. Brown Jr., G. A. Waychunas, A. C. Chaka, and T. P. Trainor, Surf. Sci. **601**, 460 (2007).

[16] G. Kresse, J. Hafner, Phys. Rev. B **48**, 13115 (1993); G. Kresse and J. Furthmuller, Comput. Mater. Sci. **6**, 15 (1996).

[17] P. E. Blöchl, Phys. Rev. B **50**, 17953 (1994); G. Kresse and D. Joubert, Phys. Rev. B **59**, 1758 (1999).

[18] J. P. Perdew, K. Burke, and M. Ernzerhof, Phys. Rev. Lett. **77**, 3865 (1996).

[19] H. J. Monkhorst and J. D. Pack, Phys. Rev. B **13**, 5188 (1976).

[20] M. Methfessel and A. T. Paxton, Phys. Rev. B **40**, 3616 (1989).

[21] R. E. Newnham and Y. M. de Haan, Zeits. Kristallogr. **117**, 235 (1962); R. L. Blake, R. E. Hessevick, T. Zoltai, and L. W. Finger, Am. Mineral. **51**, 123 (1966).

[22] A. Kirfel and K. Eichhorn, Acta Crystallogr. A **46**, 217 (1990).

[23] B. Z. Lodziana, J. K. Norskov, and P. Stoltze, J. Chem. Phys. **118**, 111979 (2003)

[24] C. Wolverton and K. Hess, Phys. Rev. B **63**, 024102 (2001).

[25] J. M. D. Coey and G. A. Sawatzky, J. Phys C: Solid State Phys. **4,** 2386 (1971); E. Kren, P. Szabo, and G. Konczos, Phys. Lett. **19**, 103 (1965).

[26] D. D. Sarma, N. Shanthi, S. R. Barman, N. Hamada, H. Sawada, and K. Terakura, Phys. Rev. Lett. **75**, 1126 (1995); L. M. Sandratskii, M. Uhl, and J. Kübler, J. Phys.: Condens. Matter **8,** 983 (1996); X.-G. Wang, W. Weiss, S. K. Shaikhutdinov, M. Ritter, M. Petersen,

F. Wagner, R. Schlögl, and M. Scheffler, Phys. Rev. Lett. **81**, 1038 (1998); A. Rohrbach, J. Hafner, and G. Kresse, Phys. Rev. B **70**, 125426 (2004).

[27]K. Reuter and M. Scheffler, Phys. Rev. B **65**, 035406 (2002); X.-G. Wang, A. Chaka, and M. Scheffler, Phys. Rev. Lett. **84**, 3650 (2000).

[28]Q. Sun, K. Reuter, and M. Scheffler, Phys. Rev. B **67**, 205424 (2003).

[29]*NIST-JANAF Thermochemical Tables*, 4th ed., edited by J. M. W. Chase (American Chemical Society, Washington, DC, 1998).

[30]I. D. Brown and D. Altermatt, Acta Crystallogr. B **41**, 244 (1985).

[31]J. R. Barger, S. N. Towle, G. E. Brown Jr., and G. A. Parks, J. Colloid Interface Sci. **185**, 473 (1997).

[32]G. Henkelman, A. Arnaldsson, and H. Jónsson, Comput. Mater. Sci. **36**, 254 (2006); E. Sanville, S. D. Kenny, R. Smith, and G. Henkelman, J. Comp. Chem. **28**, 899 (2007); W. Tang, E. Sanville, and G. Henkelman, J. Phys.: Condens. Matter **21**, 084204 (2009).

[33]G. Pacchioni, J. Chem. Phys. **128**, 182505 (2008).

[34]A. L. Allred, J. Inorg. Nucl. Chem. **17**, 215 (1961).

[35]I. D. Brown, *The Chemical Bond in Inorganic Chemistry: The Bond Valence Model* (Oxford University Press, New York, 2002).

[36]G. V. Gibbs, D. F. Cox, M. B. Bolsen Jr., R. T. Downs, and N. L. Ross, Phys. Chem. Minerals **30**, 305 (2003); G. V. Gibbs, D. F. Cox, N. L. Ross, T. D. Crawford, J. B. Burt, and K. M. Rosso, Phys. Chem. Minerals **32**, 208 (2005).